*Int. J. Electrochem. Sci.*, 12 **(2017)** 9040 – 9050, doi: 10.20964/2017.10.87

**International Journal of ELECTROCHEMICAL SCIENCE**
www.electrochemsci.org

# Preparation of Metal Nanoparticles by Jet Electrodeposition Using Monocrystalline Silicon Substrate

*Lida Shen*[1,*], *Wei Zhuo*[1], *Mingbo Qiu, Zongjun Tian, Chuan Wang*

College of Mechanical and Electrical Engineering, Nanjing University of Aeronautics and Astronautics, Nanjing, 210016
[1] These authors contributed equally to this work
[*]E-mail: ldshen@nuaa.edu.cn

*Received:* 5 July 2017 / *Accepted:* 18 August 2017 / *Published:* 12 September 2017

This study proposes a method for rapid preparation of nanoparticles (NPs) by jet electrodeposition on silicon substrate. Micropyramidal structures were formed on a specific crystallographic plane of monocrystalline silicon substrate after polishing and alkali treatment. With cathode translational motion and high current density, jet electrodeposition discharged metal ions into atoms that rapidly assembled at the tip of silicon micropyramids to form nuclei and generate NPs. The effects of surface roughness, current density, and cathode translational speed on NP size and distribution uniformity were investigated by using copper NPs as the research object. NP size distribution rules for different parameters were obtained by the field emission scanning electron microscopic image analysis and optimized process parameters. Results showed that low silicon substrate roughness was favored preparation of copper NPs with good size refinement and uniform size distribution. Moreover, these NPs exhibited desirable refinement and uniformity when the current density was 200 A/dm$^2$ and cathode translational speed 480 mm/min.

**Keywords:** jet electrodeposition; nanoparticles; surface roughness; current density; cathode translational speed

## 1. INTRODUCTION

Metal nanoparticles (NPs) belong to zero-dimensional nanomaterials and possess the basic properties of small scale, surface, quantum size, and quantum tunneling effects. This material has many properties that differ from conventional materials of the same composition and shows numerous distinct behaviors and significant potential applications in various fields, such as in mechanics, electricity, magnetism, and chemistry [1–4]. Research into NP preparation is the basis of NP developments, including nanotechnology. NPs are prepared mainly by solid-state reactions, gas-phase

methods, and liquid phase methods. Typical processing methods are high-energy ball milling [5–7], gas evaporation [8–9], and hydrothermal methods [10–11]. However, existing preparation methods are expensive and tedious, thus making metal NPs expensive and restrict their development and applications.

In view of the above problems, a method for preparing metal NPs by jet electrodeposition using monocrystalline silicon substrate was proposed. As a branch of electrodeposition, jet electrodeposition has high material transfer rate and high limiting current density [12–15], which can obtain copper film with grain sizes between 30–80 nm over a large current density range [16–17]. Monocrystalline silicon appears to be arranged evenly in pyramidal microstructures oriented in the same direction after alkali corrosion [18–20]. Combined with these characteristics, this study addressed the rapid preparation of copper NPs on monocrystalline silicon surfaces by jet electrodeposition. Compared with conventional preparation methods of metal NPs, this technology did not require tedious procedures and costly equipment and was also faster and not harmful to humans or the environment. Thus, implementation of this technology was simple, stable, and easy to control. Here, the production of copper NPs with fine particle size and uniform distribution was studied by investigating the deposition process and optimizing the process parameters.

## 2. EXPERIMENTAL

### *2.1 Experimental device*

The system principle adopted in this experiment is shown in Fig. 1. Under different process parameters, this device can adjust the nozzle exit width, translational speed of workpiece, and cathode current density to prepare nanometal particles with different dimensions. The method was based on an embedded control system to allow automatic control of the jet electrodeposition process. During the cathode back-and-forth translational movement, discharged ions deposited on the tips of silicon substrate micropyramid structures. As a result, tiny crystal nuclei formed that, in turn, grew into copper NPs.

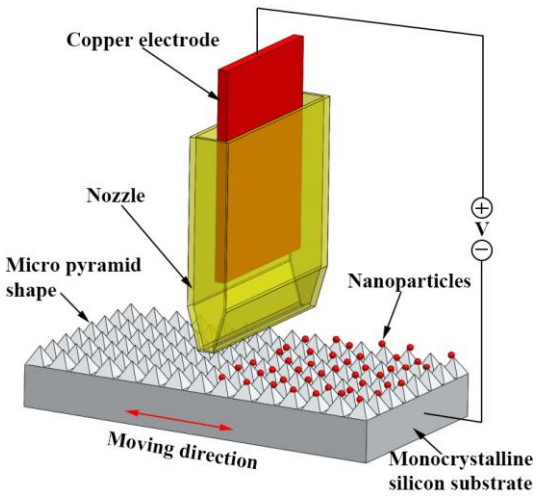


**Figure 1.** Principle diagram of the jet electrodeposition of copper nanoparticles

A diagram of the jet electrodeposition experimental device and a scene photograph are shown in Figs. 2 and 3, respectively. The workpiece translation system was composed of the machine tool main body, power control system, electrolyte circulation system, step motor control system, and sedimentary units. A workpiece was installed on the fixture and reciprocating movements under step motor control. Electrolyte flowing from the nozzle at high speed completed the anode (copper) and cathode (silicon) circuit. Under the high current density provided by the power system, copper ions were selectively deposited on the silicon substrate surface.

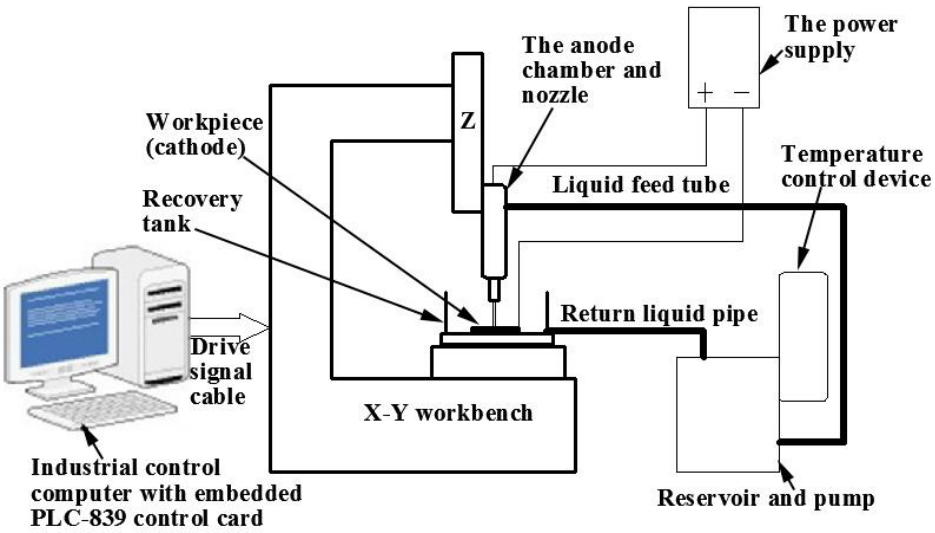


**Figure 2.** Diagram of the jet electrodeposition experimental device

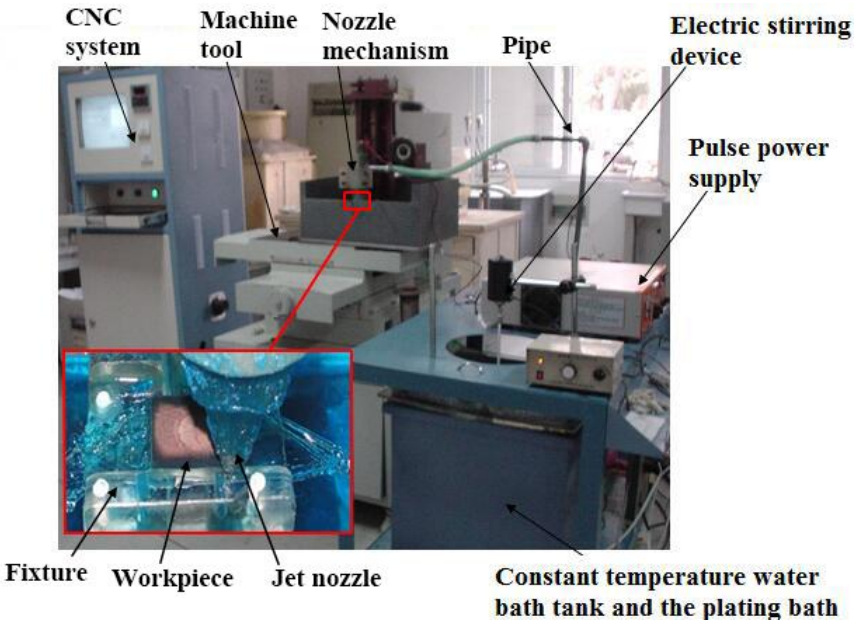


**Figure 3.** Scene photograph of the jet electrodeposition system

*2.2 Establishment of process test*

The electrolyte composition of electrodeposited copper is shown in Table 1.

**Table 1.** Electrolyte composition.

| Solution composition | Content (g/L) |
|---|---|
| $CuSO_4 \cdot 5H_2O$ | 240 |
| $H_2SO_4$ | 50 |
| Additive (phenolsulfonic acid, glucose) | A little |

Alkaline etching of monocrystalline silicon, also called surface texturing of monocrystalline silicon, is an important step in the preparation of solar panels, and the process is quite mature. Through consulting relevant documents [21–22], this experiment used (100) oriented monocrystalline silicon (Cz, p-type, 1–10 Ω·cm) as the substrate, which was 20×20×1 mm in size. Grinding and polishing were used for substrate mechanical pretreatment. The solution formula for substrate alkaline etching and the experimental process parameters are shown in Tables 2 and 3, respectively.

**Table 2.** Solution formula for alkaline etching of monocrystalline silicon.

| Solution composition | Content (%) | Temperature (°C) | Time (min) | Effect |
|---|---|---|---|---|
| NaOH | 2 | 85 | 40 | Etch silicon wafer |
| IPA ($C_3H_8O$) | 15 | | | Remove hydrogen bubbles |

**Table 3.** Process parameters.

| Process parameters | Parameter values | Process parameters | Parameter values |
|---|---|---|---|
| Machining polarity | Workpiece is negative | Scanning times | 1 |
| Surface roughness (μm) | 0.017/0.160 | Section sizes of nozzle | 20×0.5 mm |
| Current density ($A/dm^2$) | 100/200/300/400 | Machining gap (mm) | 2 |
| Cathode translational speed (mm/min) | 120/240/360/480 | The speed of electrolyte (m/s) | 1 |

## 3. RESULTS AND DISCUSSION

*3.1 Mechanism analysis of copper NPs prepared by jet electrodeposition*

The basic principles of metal electrodeposition are nucleation and crystallization. The process of electrical crystallization comprises metal ion discharge and lattice growth. Meanwhile, the properties of the obtained metal nanoparticles were directly influenced by various parameters, such as

current density, electrode potential, translational speed of cathode, electrolyte composition, and any additive.

*3.1.1 Surface morphology of monocrystalline silicon after etching*

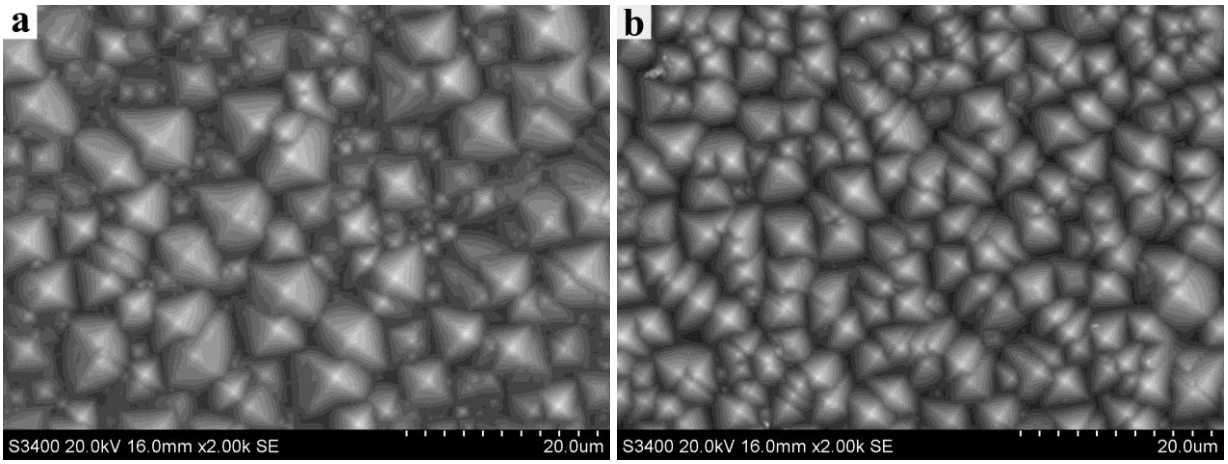


**Figure 4.** SEM images of monocrystalline silicon with different roughness after etching: (a) 0.160 μm, (b) 0.017 μm

Scanning electron microscopic (SEM) images of monocrystalline silicon (silicon wafers) with different roughness after etching showed many surface pyramidal microstructures (Fig. 4). These structures resulted because the monocrystalline silicon was anisotropic when it was corroded in alkaline solution within a certain concentration range [22], which allowed a $OH^-$ reaction rate with the silicon (100) plane that was several times or even dozens of times faster than with (111). The corrosion reaction started on the (100) plane and finally exposed the (111) plane, which resulted in numerous quadrilateral cones on the silicon surface, commonly known as "pyramid" structures. The alkali corrosion reaction with monocrystalline silicon at high temperature occurred as follows:

$$2NaOH + Si + H_2O \rightarrow Na_2SiO_3 + 2H_2\uparrow$$

*3.1.2 Microdeposition of different substrates*

As a partial electrodeposition technology, each nozzle scanning movement was helpful in forming a new discharge point on the deposited layer and high current density also guaranteed the nucleation rate and density [23]. Then, a new crystal nuclei was formed easily on the substrate surface under the influence of the tip discharge effect. It was found that metal NPs produced on the silicon substrate surface were easily displaced by hand. Thus, to facilitate characterization of the results, copper NPs were obtained by lifting the particles off the substrate with a SEM special conductive adhesive tape, and particle morphology characterized by field emission (FE) SEM.

Under the same processing parameters, the deposit morphologies of different substrates showed that, with sheet copper used as the cathode substrate, the deposited layer formed a compact copper film (Fig. 5a1).

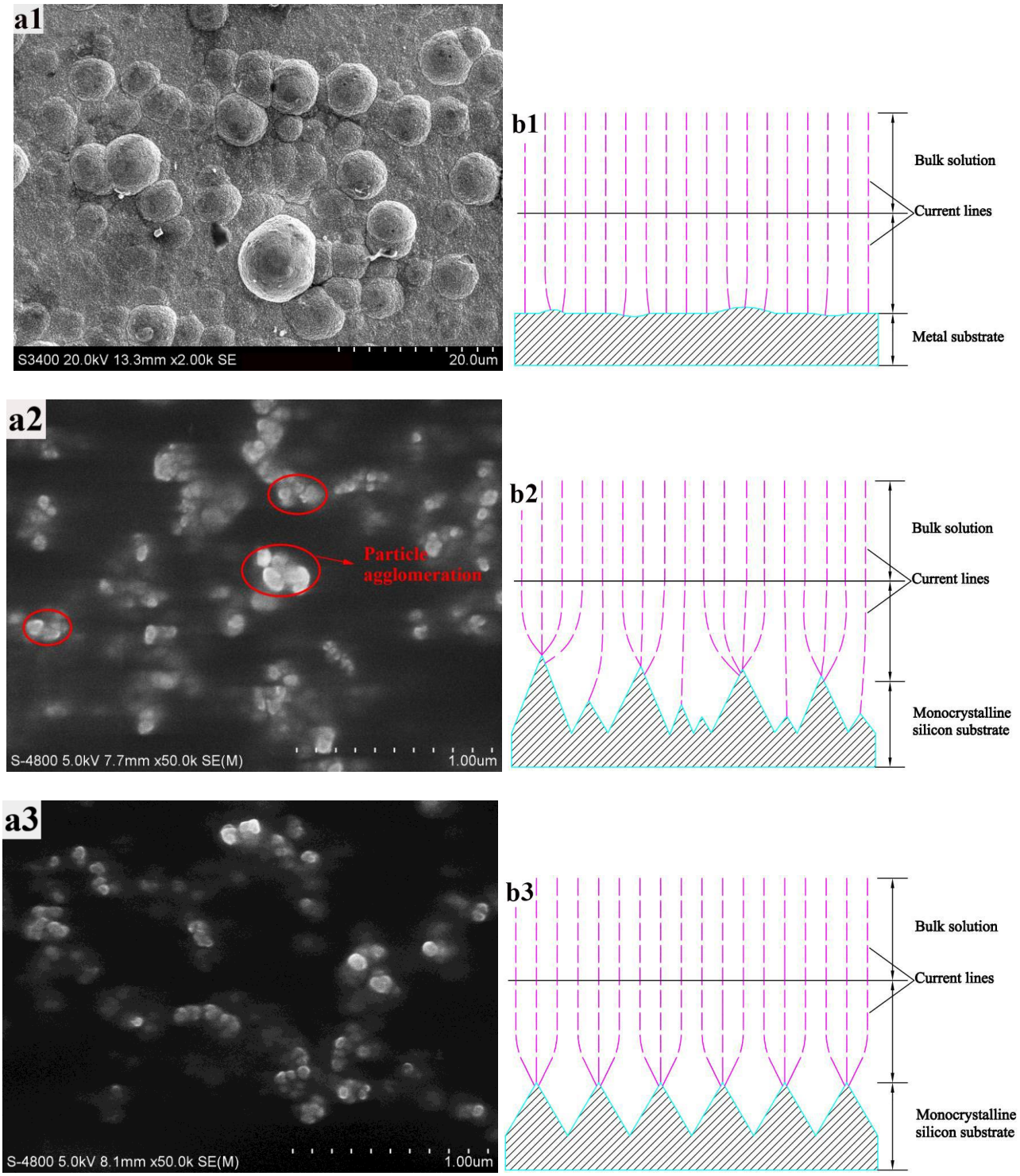


**Figure 5.** Microdeposition process and power line distribution of different substrates: (a1) Sheet copper substrate, (b1) Power line distribution of metal substrate, (a2) Ra = 0.160 μm monocrystalline silicon substrate, (b2) Power line distribution of large roughness monocrystalline silicon after corrosion, (a3) Ra = 0.017 μm monocrystalline silicon substrate, (b3) Power line distribution of low roughness monocrystalline silicon after corrosion

However, when monocrystalline silicon with its pyramidal structures was used as the substrate, the deposition layer was composed of dispersed copper NPs (Figs. 5a2–5a3). Also, with decreased silicon substrate roughness before etching, finer and more uniform copper NPs were obtained.

Electrocrystallization consists of three steps: formation of adsorption ions, diffusion of ions on the cathode surface, and entrance into the crystal lattice when ions reach the growing points [24]. Generally, the growing points are surface defects, such as edges and steps [14]. Compared to the etched monocrystalline silicon surface, a polished sheet copper substrate surface was much flatter. Although the sheet copper surface possessed some defects, such as micro-bulges and holes, they only caused uneven distribution of local power lines. As a whole, the distribution of power lines was relatively uniform (Fig. 5b1), such that the nucleation and growth of copper ions occurred on the entire substrate surface and formed a copper film. However, the surface of etched monocrystalline silicon showed many pyramidal microstructures (Fig. 4), and the existence of these pyramids allowed them to be the growth points for copper ion discharge. At the same time, because of these substrate microstructures, a large number of cutting-edge advantages could be exploited during electrodeposition. As the power line was concentrated at the pyramid tips (Figs. 5b2–5b3), impetus was provided for nucleation and growth of copper atoms at the tips. The discharge of $Cu^{2+}$ in the electrolyte resulted in Cu atom formation and rapid grain formation. Thus, dispersed nanometer copper particles were generated.

The copper NPs deposited on etched monocrystalline silicon with an initial roughness of 0.160 μm were larger and appeared seriously agglomerated (Fig. 5a2), while substrate with lower roughness formed finer and more uniform NPs (Fig. 5a3). These results were because, as the roughness of the substrate decreased, the surface was flatter and more favorable for the formation of uniform and highly consistent surface pyramid morphology after alkaline etching (Fig. 4b). Thus, under the influence of these effects, the concentration of power lines at the many pyramid tips was even more uniform (Fig. 5b3). At high current densities, the many available tips allowed ion discharges to produce finer nuclei at the tips, and the nuclei rapidly gathered around the tips to produce NPs of good quality. As the effects of using substrate with roughness of 0.017 μm produced very good results, the following experiments were performed using such substrates.

### *3.2 Influence of current density on particle size and uniformity*

The particle size distribution of copper NPs prepared under different current densities, with the cathode translational speed held at 240 mm/min, showed that, with increased current density, the size and distribution of NPs first improved and then deteriorated (Fig. 6).

Winand [25] has argued that the entire process of crystal growth is related to the deposition overpotential. The nucleation probability $W$ and the overpotential $\eta_k$ exhibit the following relationship:

$$W = B \cdot \exp(-b/\eta_k^{\,2})$$

with $B$ and $b$ being constants. The higher the crystallization overpotential was, the higher the probability of crystal nuclei formation. Accordingly, the number of crystal nuclei was higher and crystal nucleus size smaller, such that the NP size was refined. Furthermore, the main factor that

affected the overpotential was current density [26]. With high current density during jet electrodeposition, the overpotential was increased and, as a result, the crystal nuclei formation speed was improved and crystal nucleus size refined [27]. With increased current density, the electric field intensity was stronger and the distribution of power lines more concentrated per unit time and unit area. Therefore, in the crystallization process, more copper ions passed through the double layer and adsorbed onto the substrate surface, forming more nuclei and producing fine copper NPs (Fig. 6b). When the current density was 300 A/dm$^2$, finer and more numerous NPs were observed, such that the probability of agglomeration was greater (Fig. 6c). When the current density was increased to 400 A/dm$^2$, particle size became larger and agglomeration worse (Fig. 6d), which was because the current density was too high, resulting in increased polarization. Also, the electrolyte did not provide sufficient metal ions for the electrodeposition process, such that nuclei that were formed grew further and particle size thus increased. The above analysis showed that increased current density had a significant effect on the NP size, and excessive current density caused NP aggregation.

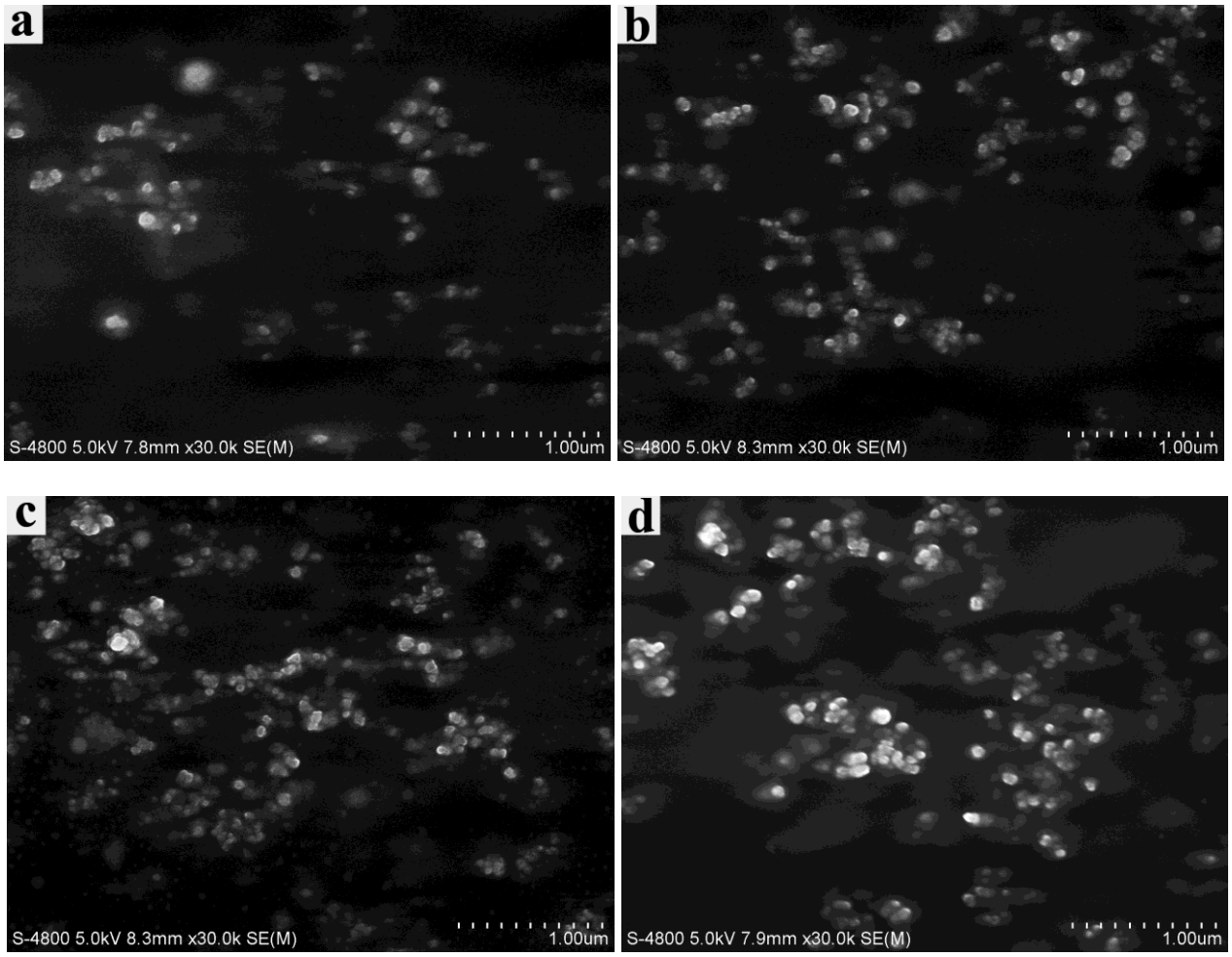


**Figure 6.** Particle size distribution of copper NPs under different current densities: (a) 100 A/dm$^2$, (b) 200 A/dm$^2$, (c) 300 dm$^2$, (d) 400 dm$^2$

When the current density was 200 A/dm$^2$, the size and uniformity of the resulting NPs was quite good. Compared with the conventional electrodeposition of preparing NPs [28-30], the current

density used by this method is scores of times higher than those methods, which makes up the defect of the slow speed of metal NPs prepared by electrodeposition.

*3.3 Influence of translational speed of cathode on particle size and uniformity*

The particle size distribution of copper NPs prepared under different cathode translational speeds, with the current density at 200 A/dm$^2$, showed that, with increased translational speed, the size and distribution of NPs gradually improved (Fig. 7).

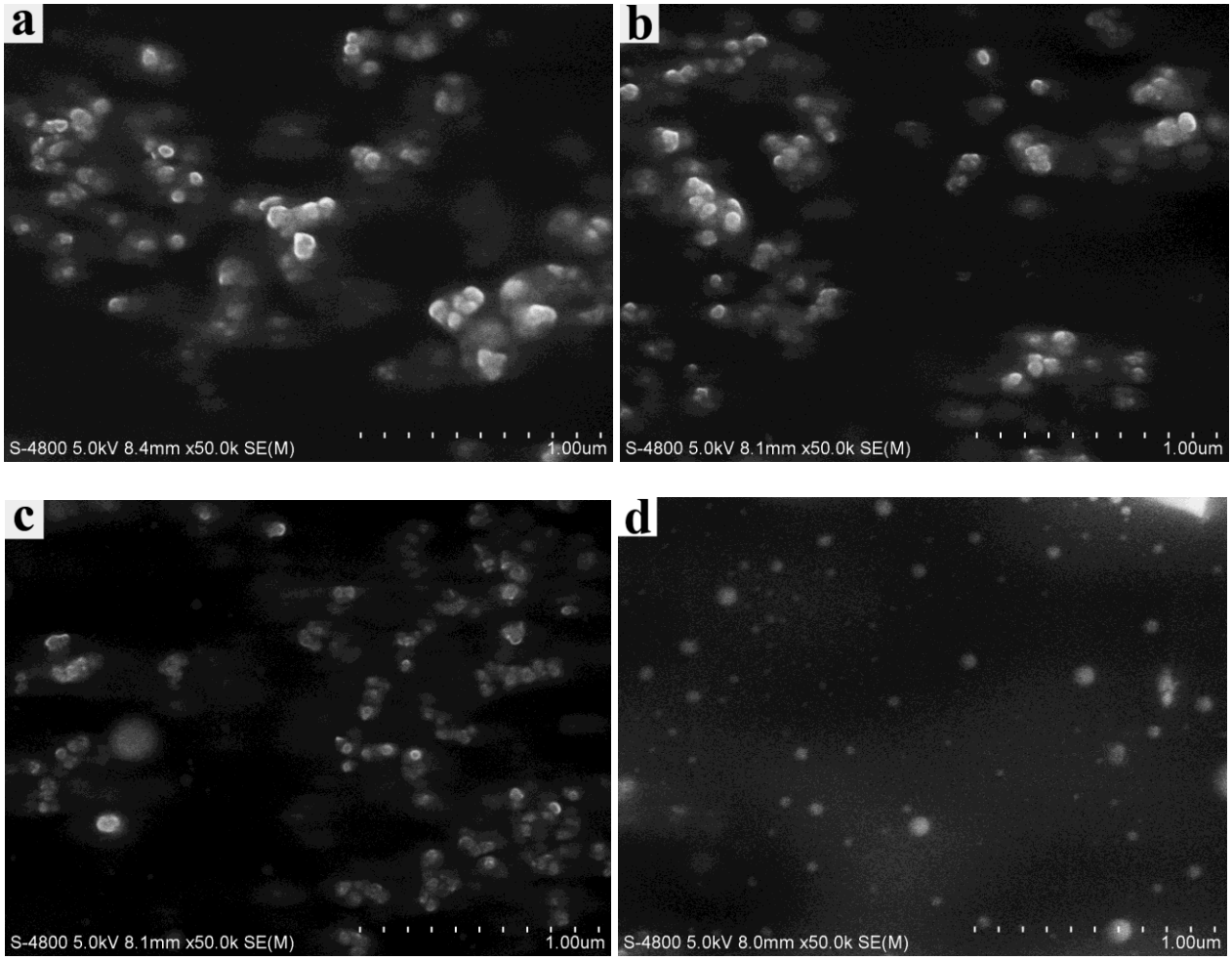


**Figure 7.** Particle size distribution of copper NPs under different cathode translational speeds: (a) 120 mm/min, (b) 240 mm/min, (c) 360 mm/min, (d) 480 mm/min

The key steps in the electrodeposition process were the generation of new crystal nuclei and then crystal growth [31]. The cathode translational speed directly influenced nucleation growth time and thus affected NP size. When the translational speed was 120 mm/min, NPs were basically agglomerated and NPs scattered (Fig. 7a). At 240 mm/min, particle size was clearly reduced, and the NP number increased, compared with the lower speed (Fig. 7b). At 360 mm/min, the particle size was further reduced and the distribution uniform (Fig. 7c), which was because the increased translation speed resulted in shorter nuclei growth times that thus refined the particle size. At 480 mm/min, the number of particles clearly decreased (Fig. 7d), the main reason for which was that the speed was too

high. In this case, the deposition time per unit area was short, such that the electric power during crystallization process was insufficient and initiated surface nuclei did not have time to grow larger. The above analysis further showed that metal NPs of different sizes could be obtained by controlling jet electrodeposition processing parameters. As a kind of local electrodeposition technique, the selective deposition is the advantage of jet electrodeposition [32]. Different from the other electrodeposition method complexity [33], in the full use of the advantages of jet electrodeposition and pyramid structures of monocrystalline silicon after alkali corrosion, electrodeposition method to prepare metal NPs becomes easier and more controllable.

## 4. CONCLUSIONS

(1) Copper NPs with good properties were obtained by jet electrodeposition technology, with optimized process parameters, using monocrystalline silicon substrate pretreated by polishing and alkali etching.

(2) The lower the silicon wafer roughness was, the better the NPs prepared, using etched silicon as the substrate. When the roughness was 0.017 μm, the NP particle size was fine and the size distribution relatively uniform.

(3) With increased current density, nucleation rates improved and crystal nuclei become smaller and, consequently, particle size diminished. However, if current density was increased above a certain threshold, particle agglomeration occurred. When the current density was 200 $A/dm^2$, the size and uniformity of the prepared particles were good.

(4) The crystallization process was directly affected by the cathode translational speed. With increased translational speed, the deposition time per unit area was shortened and the power insufficient; this phenomenon led to particle dispersion and thinning. At 480 mm/min, the NPs obtained were fine in size and uniform in distribution.

ACKNOWLEDGEMENTS
This project is supported by the NUAA Fundamental Research Funds (NS2014053). The authors also extend their sincere thanks to those who contributed in the preparation of the instructions.

## References

1. J. Tian, D. F. Peng, X. Wu, W. Li, H. B. Deng, S. L. Liu, *Carbohyd. Polym*., 156 (2017) 19.
2. V. Bonfrate, D. Manno, A. Serra, L. Salvatore, A. Sannino, A. Buccolieri, T. Serra, G. Giancane, *J. Colloid. Interf. Sci*., 501 (2017) 185.
3. Y. T. Zhao, C. H. Jiang, Z. Xu, F. Cai, Z. Q. Zhang, P. Fu, *Mater. Design*., 85 (2015) 39.
4. S. L.Viñas, K. Simeonidis, Z. A. Li, Z. Ma, E. Myrovali, A. Makridis, D. Sakellari, M. Angelakeris, U. Wiedwald, M. Spasova, M. Farle, *J. Magn. Magn. Mater*., 415 (2016) 20.
5. S. Amirkhanlou, M. Ketabchi, N. Parvin, *Mater. Lett*., 86 (2012) 122.
6. S. Fathinia, M. Fathinia, A. A. Rahmani, A. Khataee, *Appl. Surf. Sci*., 327 (2015) 190.
7. B. F. Amorim, M. A. Morales, F. Bohn, A. S. Carriço, S. N. de Medeiros, A. L. Dantas, *Physica.*

B., 488 (2016) 43.
8. F. Yılmaz, D. J. Lee, J. W. Song, H. S. Hong, H. T. Son, J. S. Yoon, S. J. Hong, *Powder. Technol.*, 235 (2013) 1047.
9. T. Fujimoto, S. Ogawa, T. Kanai, N. Uchiyama, T. Yoshida, S. Yagi, *Int. J. Hydrogen. Energ*., 40 (2015), 11890.
10. C. S. Bezerra, M. E. G. Valerio, *Physica.* B., 501 (2016) 106.
11. S. Fuentes, P. Muñoz, J. Llanos, M. Vega, I. R. Martin, E. Chavez-Angel, *Ceram. Int*., 43 (2017) 3623.
12. Z. J. Tian, D. S. Wang, G. F. Wang, L. D. Shen, Z. D. Liu, Y. H. Huang, T. *Nonferr. Metal. Soc.*, 20 (2010) 1037.
13. G. F. Wang, L. D. Shen, Y. H. Huang, *Int. J. Electrochem. Sci*., 7 (2012) 10818.
14. X. Liu, L. D. Shen, M. B. Qiu, Z. J. Tian, Y. H. Wang, K. L. Zhao, *Surf. Coat. Tech*., 305 (2016) 231.
15. D. Z. Huang, L. D. Shen, J. S. Chen, J. Zhu, *Trans. Indian. Inst. Met*., 67 (2014) 351.
16. Y. P. Zhao, Y. H. Huang, Z. D. Liu, Z. J. Tian, J. F. Zhao, *electromachining & Mould*. 5 (2004) 26.
17. Y. P. Zhao, Y. H. Huang, J. W. Zhang, Z. D. Liu, Z. J. Tian, J. F. Zhao, G. R. Hua, *Mater. Mech. Eng*., 30 (2006) 87.
18. D. Z. Dimitrov, C. H. Du, *Appl. Surf. Sci*., 266 (2013) 1.
19. B. Vallejo, M. González-Mañas, J. Martínez-López, M. A. Caballero, *Sol. Energy*., 81 (2007) 565.
20. P. K. Basu, H. Dhasmana, N. Udayakumar, F. Khan, D. K. Thakur, *Sol. Energ. Mat. Sol. C*., 94 (2010) 1049.
21. H. L. Li, L. Zhao, H. W. Diao, C. L. Zhou, W. J. Wang, *J. Synthetic. Cryst.*, 39 (2010) 857.
22. Y. Nishimoto, K. Namba, *Sol. Energ. Mat. Sol*. C., 61 (2000) 393.
23. Y. H. Wang, L. D. Shen, M. B. Qiu, Z. J. Tian, X. Liu, W. Zhuo, *J. Electrochem. Soc.*, 163 (2016) 579.
24. B. Lv, Z. F. Hu, X. H, Wang, B. S. Xu, Chin. *J. Mater. Res.*, 4 (2014) 255.
25. R. Winand, *Electrochim. Acta.*, 39 (1994) 1091.
26. Y. Xiong, T. F. Jing, G. Y. Qiao, G. J. Shao, S. X. Yu, *Electroplat & Finishing*. 5 (2000) 1.
27. D. S. Wang, Y. H. Huang, Z. J. Tian, Z. D. Liu, J. Zhu, *Mater. Mech. Eng.*, 2 (2008) 53.
28. F. Pagnanelli, P. Altimari, M. Bellagamba, G. Granata, E. Moscardini, P. G. Schiavi, L. Toro, *Electrochim. Acta.*, 155 (2015) 228.
29. D. Z. Zhang, Y. Tang, F. G. Jiang, Z. H. Han, J. Chen, *Appl. Surf. Sci.*, 369 (2016) 178.
30. I. Golvano-Escobala, S. Suriñacha, M. D. Baróa, S. Panéb, J. Sortc, E. Pellicera, *Electrochim. Acta.*, 194 (2016) 263.
31. B. Lv, Z. F. Hu, X. H. Wang, B. S. Xu, *Surf. Coat. Tech.*, 270 (2015) 123.
32. L. D. Shen, Y. H. Wang, W. Jiang, X. Liu, C. Wang, Z. J. Tian, *Corros. Eng. Sci. Techn.*, 52 (2017) 311.
33. S. Javadian, J. Kakemam, A. Sadeghi, H. Gharibi, *Surf. Coat. Tech.*, 305 (2016) 41.